Bioorganic & Medicinal Chemistry Letters 20 (2010) 2586–2590

Contents lists available at ScienceDirect

Bioorganic & Medicinal Chemistry Letters

journal homepage: www.elsevier.com/locate/bmcl

Novel benzofuran-3-one indole inhibitors of PI3 kinase-α and the mammalian target of rapamycin: Hit to lead studies

Matthew G. Bursavich [a], Natasja Brooijmans [b], Lawrence Feldberg [c], Irwin Hollander [c], Stephen Kim [c], Sabrina Lombardi [a], Kaapjoo Park [a], Robert Mallon [c], Adam M. Gilbert [a,*]

[a] Medicinal Chemistry, Chemical Sciences, Wyeth Research, Pearl River, NY 10965, USA
[b] Computational Chemistry, Chemical Sciences, Wyeth Research, Pearl River, NY 10965, USA
[c] Discovery Oncology, Wyeth Research, Pearl River, NY 10965, USA

ARTICLE INFO

Article history:
Received 17 January 2010
Revised 18 February 2010
Accepted 19 February 2010
Available online 23 February 2010

Keywords:
Kinase
Phosphatidylinositol-3-kinases
Mammalian target of rapamycin

ABSTRACT

A series of benzofuran-3-one indole phosphatidylinositol-3-kinases (PI3K) inhibitors identified via HTS has been prepared. The optimized inhibitors possess single digit nanomolar activity against p110α (PI3K-α), good pharmaceutical properties, selectivity versus p110γ (PI3K-γ), and tunable selectivity versus the mammalian target of rapamycin (mTOR). Modeling of compounds **9** and **32** in homology models of PI3K-α and mTOR supports the proposed rationale for selectivity. Compounds show activity in multiple cellular proliferation assays with signaling through the PI3K pathway confirmed via phospho-Akt inhibition in PC-3 cells.

Phosphatidylinositol-3-kinases (PI3K) are lipid kinases that phosphorylate the 3′-hydroxyl position of phosphatidylinositol 4,5-diphosphate (PIP2) to phosphatidylinositol 3,4,5-triphosphate (PIP3). Eight PI3Ks have thus far been identified and categorized into four classes (IA, IB, II and III) based on substrate specificity and sequence homology. Deregulation of class IA PI3Ks, namely p110α (PI3K-α), leads to elevated PIP3 levels and downstream activation of Akt.[1,2] This ultimately promotes growth, survival, proliferation, enhanced migration, and adhesion in cancer cells. Additionally, PI3K-α deregulation is involved a quarter of breast cancers in all stages. Also, PTEN (the phosphatase that regulates PIP3 levels) deregulation is associated with resistance to chemotherapeutic agents that target the EGFR/Her2 signaling pathway.[3,4] Thus PI3K-α has emerged as a premier target for cancer treatment and the focus of many drug discovery efforts.[5]

A high-throughput screen of our compound library identified a series of benzofuran-3-one indoles (Fig. 1) with activity against PI3K-α, p110γ (PIK3-γ), a related PI3K subtype (class IB) targeted for autoimmune and inflammation diseases,[6] and the mammalian target of rapamycin (mTOR), a related kinase targeted in cancer chemotherapy that signals downstream of Akt.[7] Since many of the effects of Akt are mediated via mTOR, a dual PI3K/mTOR inhibitor has the potential to prevent cancer cell proliferation and induce apoptosis by fully suppressing Akt activation.

We have recently published our efforts developing purines and pyrazolo[3,4-*d*]pyrimidines as selective inhibitors of both PI3K-α and mTOR.[8,9] Herein we report the hit to lead optimization and structure–activity relationships (SAR) of benzofuran-3-one indoles, another class of novel PI3K-α inhibitors with good selectivity versus PI3K-γ and mTOR.

The synthesis of the benzofuran-3-one indole inhibitors is shown in Scheme 1.[10] The synthesis begins with commercially available indoles **2** or their construction from **1** via standard Suzuki cross-coupling conditions.

Indoles **2** were formylated with $POCl_3$ in DMF to give **3**.[11] In some instances, the indole nitrogens of **3** were methylated with MeI using NaH in DMF.[12] Condensation of 4,6-dihydroxybenzofuran-3(2*H*)-one **4** with indoles **3** under catalytic acid conditions provided the desired benzofuran-3-one indoles **5**.[13]

Compounds were assayed using PI3K-α and PI3K-γ fluorescence polarization assays to monitor PIP3 production. Compounds were further assayed for mTOR potency using the DELFIA format

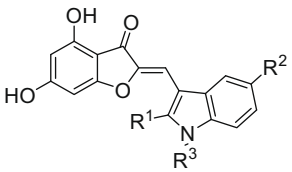

Figure 1. Benzofuran-3-one indole PI3K inhibitor scaffold identified via HTS.

* Corresponding author. Tel.: +1 845 602 4865; fax: +1 845 602 5561.
E-mail address: gilbera@wyeth.com (A.M. Gilbert).

0960-894X/$ - see front matter © 2010 Elsevier Ltd. All rights reserved.
doi:10.1016/j.bmcl.2010.02.082

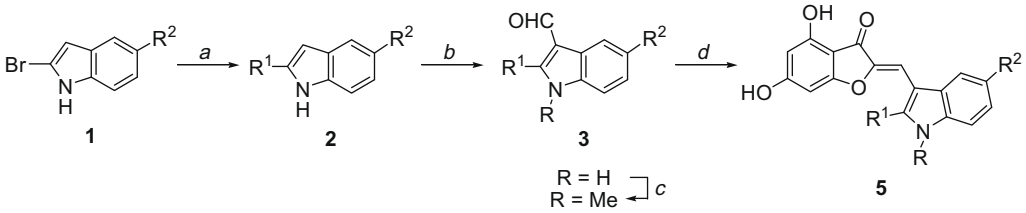

Scheme 1. Reagents and conditions: (a) $R^1B(OH)_2$, Na_2CO_3, cat. $Pd(PPh_3)_4$, dioxane, reflux; (b) $POCl_3$, DMF, 0–23 °C; (c) MeI, NaH, DMF; (d) 4,6-dihydroxybenzofuran-3(2*H*)-one, cat. HCl, EtOH, reflux.

monitoring phosphorylated His6-SK6. Cellular proliferation activity was determined by monitoring cell growth densities in Caco2, LoVo, and PC3MM2 cell cultures.[14] Mechanism based cellular assays of PI3K signaling in PC-3 cells was determined by immunoblotting protein lysates for phosphorylated-Akt (p-Akt) and phosphorylated 4E binding protein 1 (p-4EBP1).

The 5-indole (R^2) substituent was initially varied while maintaining the R^1 substituent as a proton, methyl, or aryl group (Table 1). The importance of the R^2 substituent was evident in the early analogs where R^1 = H. Changing R^2 to a halogen (**7** and **8**) gives a significant PI3K-α potency improvement over **6** with at least five-fold selectivity versus PI3K-γ and mTOR. Incorporation of an

Table 1
Structure–activity relationships of benzofuran-3-one indoles

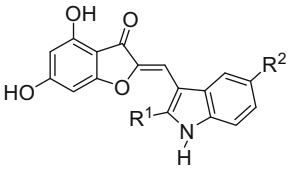

Compd	R^1	R^2	PI3K-α IC_{50}[a] (nM)	PI3K-γ IC_{50}[a] (nM)	mTOR IC_{50}[a] (nM)	Sol.[b]
6	H	H	6754	nt	9200	14
7	H	Cl	492	3628	11,000	1
8	H	Br	422	1625	3700	0
9	H	OMe	30	269	265	12
10	H	OBn	1889	nt	5000	1
11	Me	H	3197	nt	500	0
12	Me	Br	179	2220	190	1
13	Me	OMe	3	25	3	1
14	Phenyl	H	1034	2781	130	1
15	2-Pyridyl	H	3650	nt	22	3
16	(4-F)Phenyl	H	1580	nt	123	1
17	(4-Cl)Phenyl	H	542	1458	190	1
18	2-Naphthyl	H	800	1820	280	1
19	Phenyl	OMe	2	11	10	0
20	3-Pyridyl	OMe	1	10	1	1

nt = not tested.
[a] Values are means of two experiments, standard deviations are ±10%.
[b] Aqueous solubility determined at pH 7.4. Values in μg/mL.

Table 2
Structure–activity relationships of benzofuran-3-one *N*-methyl indoles

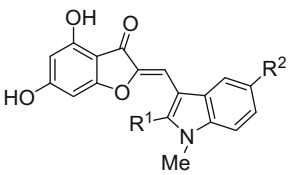

Compd	R^1	R^2	PI3K-α IC_{50}[a] (nM)	PI3 K-γ IC_{50}[a] (nM)	mTOR IC_{50}[a] (nM)	Sol.[b]
21	H	H	1106	6949	800	2
22	H	OMe	106	587	62	1
23	Me	OMe	7	54	4	1
24	Phenyl	H	2665	nt	96	2

nt = not tested.
[a] Values are means of two experiments, standard deviations are ±10%.
[b] Aqueous solubility determined at pH 7.4. Values in μg/mL.

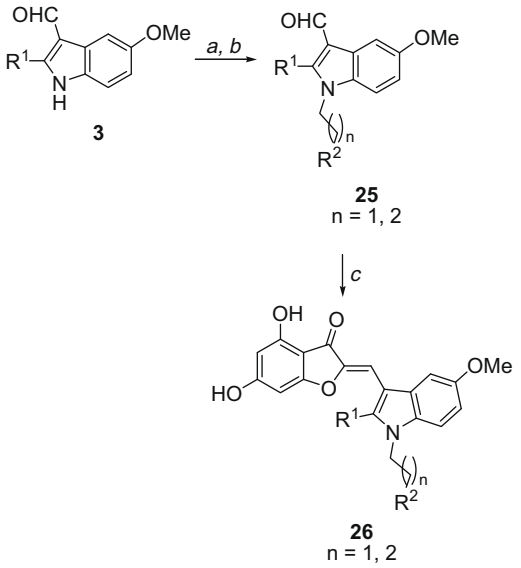

Scheme 2. Reagents and conditions: (a) $BrCH_2CH_2Cl$ or $BrCH_2CH_2CH_2Cl$, NaH, DMF; (b) amine, K_2CO_3, KI, ACN, reflux; (c) 4,6-dihydroxybenzofuran-3(2*H*)-one, cat. HCl, EtOH, reflux.

R^2 = OMe substituent in **9** further improves PI3K-α potency while maintaining 10-fold selectivity over PI3K-γ and mTOR. The R^2 = OBn analog **10** shows a substantial potency reduction compared to the corresponding OMe analog **9**. PI3K-α potency can be improved by adding an R^1 = Me substituent. While the R^2 = H analog **11** possesses low-μM PI3K-α activity, the halogenated analog **12** and the OMe-substituted **13** show significant potency increases. Compound **13** is a single digit nM PI3K-α/mTOR inhibitor with nearly 10-fold selectivity over PI3K-γ. The series of R^1 aryl substituted analogs with R^2 = H substituents (**14**–**18**) showed good mTOR potency with selectivity over both PI3K-α and PI3K-γ. As seen with the R^1 = H and Me series, R^2 = OMe analogs **19** and **20** show excellent PI3K-α potency and demonstrate selectivity versus PI3K-γ and mTOR.

Several analogs were synthesized to investigate the role of an *N*-methyl indole substituent (Table 2). The $R^1 = R^2$ = H indole **21** shows modest kinase potency. Addition of an R^2 = OMe substituent (**22**) improves potency against all three enzymes by one log unit. The R^1 = Me, R^2 = OMe analog **23** shows excellent PI3K-α and mTOR potency with nearly 10-fold selectivity over PI3K-γ. Compound **24** incorporating an R^1 phenyl group interestingly shows good mTOR potency with 26-fold selectivity over PI3K-α.

A quick look at the pharmaceutical properties of these benzofuran-3-one indoles reveals potential solubility and CYP 3A4 inhibition liabilities. For the compounds with PI3K-γ IC_{50} <100 nM (i.e., **9**, **13**, **19**, **20**, and **23**) the respective CYP 3A4% inhibition at 3 μM is 58%, 79%, 77%, 57%, and 75%. To address these potential issues and further investigate the selectivity potential, a series of indoles containing water-solubilizing groups were designed and prepared.

Construction of these benzofuran-3-one *N*-alkyl amino indoles is shown in Scheme 2.[10] The synthesis began with NaH-mediated alkylation[15] of indole **3** to provide the alkyl chloride intermediates which were then reacted with various amines to provide *N*-alkyl amino indoles **25**. Condensation of 4,6-dihydroxybenzofuran-3(2*H*)-one **4** with indole **25** under catalytic acidic conditions provided the desired benzofuran-3-one indoles **26**.[13]

Examination of the resulting benzofuran-3-one *N*-alkyl amino indoles reveals excellent PI3K-α potency and tunable PI3K-γ and mTOR selectivity (Table 3). Among the analogs containing a two carbon linker (n = 1), the R^1 = H analog **27** shows good PI3K-α potency and the greatest selectivity over mTOR. The R^1 = Me analogs (**28**–**31**) afford potent single digit nM PI3 K-α and similar mTOR potency with 10–80-fold selectivity over of PI3K-γ. All of the analogs with a three carbon linker (n = 2) and R^1 = H show good PI3K-α potency and greater than 10-fold selectivity over both PI3K-γ and mTOR. As seen previously, the corresponding R^2 methyl analogs (**35**–**38**) display more potent PI3K-α activity with 10–80-fold selectivity versus PI3K-γ and/or mTOR. Addition of the *N*-alkyl amino indoles also improves the solubility of this scaffold and moderates the CYP 3A4 liability. Among the *N*-alkyl amino indoles 27–**38** only **29**, **33** and **36** possess a CYP 3A4% inhibition at 3 μM >30% (64%, 42%, and 68%, respectively).

Table 3
Structure–activity relationships of benzofuran-3-one *N*-alkylamine indoles

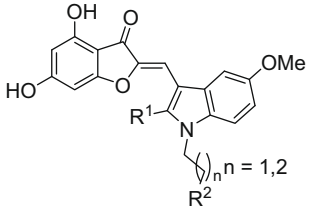

Compd	*n*	R^1	R^2	PI3K-α IC_{50}[a] (nM)	PI3K-γ IC_{50}[a] (nM)	mTOR IC_{50}[a] (nM)	Sol.[b]
27	1	H	N-$(CH_2)_2$OH piperazine	36	976	215	nd
28	1	Me	NMe_2	9	283	18	1
29	1	Me	Morpholine	11	155	9	6
30	1	Me	N-Me piperazine	5	473	11	30
31	1	Me	N-$(CH_2)_2$OH piperazine	4	322	7	30
32	2	H	NMe_2	40	2419	2125	32
33	2	H	Morpholine	42	646	430	3
34	2	H	N-$(CH_2)_2$OH piperazine	37	1358	1650	25
35	2	Me	NMe_2	5	404	118	32
36	2	Me	Morpholine	8	76	18	1
37	2	Me	N-Me piperazine	15	402	153	10
38	2	Me	N-$(CH_2)_2$OH piperazine	6	109	108	36

nd = not determined.
[a] Values are means of two experiments, standard deviations are ±10%.
[b] Aqueous solubility determined at pH 7.4. Values in μg/mL.

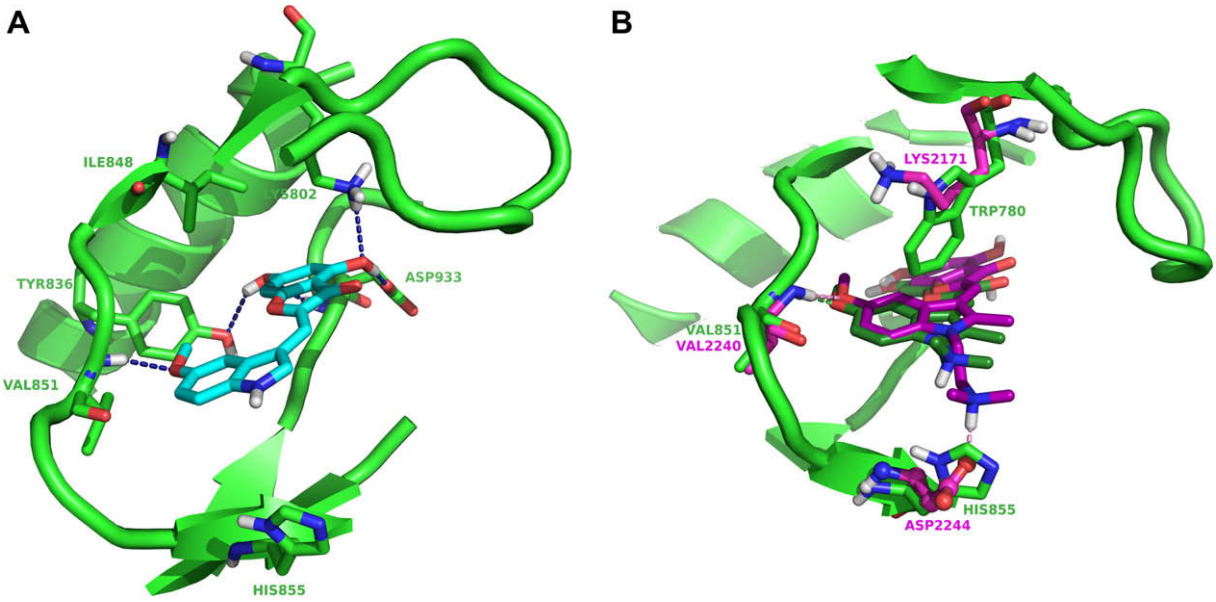

Figure 2. (A) Compound **9** docked in PI3K-α homology model. Close-up of the PI3K-α binding site in complex with **9** based on docking studies. Hydrogen bonding interactions are shown in blue dashed lines to the hinge region (Val851), the catalytic lysine (Lys802), the DFG-motif aspartic acid (Asp933), and Tyr836. The indole nitrogen points towards one of the residues in the specificity surface (His855) and solvent. (B) Overlay of docked binding modes of compound **32** in complex with PI3K-α and mTOR homology models. Overlay of the predicted binding mode of **32** with PI3K (green and dark green carbons) and mTOR (magenta and purple carbons). Hydrogen bonds are shown in green (PI3K-α) and pink (mTOR) dashed lines. The solubilizing tail cannot form hydrogen bonding interactions with the PI3K-α histidine (His855), but in mTOR can potentially form a hydrogen bond to Asp2244.

Docking models of **9** in a PI3K-α homology model (based on a published structure of PI3K-γ) and **32** in PI3K-α and mTOR homology models are shown inFigure 2A and B, respectively. The docking model of **9** reveals the 5-OMe substituent binds to the hinge region (Val851), and the OH groups bind to the catalytic lysine (Lys802), the DFG-motif aspartic acid (Asp933), and Tyr836. Docking studies of **32** show the *N*-alkylamine substituent points towards the selectivity surface and solvent. R^2 Substituents are not predicted to form hydrogen bonding interactions with the protein and these substituents thus function as solubilizing tails, with relatively little impact on potency.

In mTOR on the other hand, an aspartic acid (Asp2244) is present in the selectivity surface allowing the possible formation of a hydrogen bond with the quaternary nitrogen of the R^2 substituent (i.e., NMe_2 in **32** and **35**, morpholine in **33** and **36**). Despite the possible formation of a hydrogen bond with the enzyme, some R^2 substituents decrease potency against mTOR significantly as seen in **32**. One possible explanation for the potency decrease is that the hydrogen bond formation results in a decrease of the entropy of the substituent/inhibitor. It is also possible that the quaternary nitrogen has an electrostatic clash with Lys2171 in mTOR, which is a tryptophan in PI3K-α.

Several of the most potent PI3K-α analogs were tested for cellular proliferation activity against Caco-2 epithelial colorectal adenocarcinoma cells, LoVo human colon carcinoma cells, and PC3 human prostate cancer cells (Table 4). Inspection of the cellular data reveals the biochemical single digit nanomolar, dual PI3K-α/mTOR inhibitors trend to more promising cellular potency (compare **19**–**20** with **35**–**38**). It also appears that for the LoVo and PC3 data, the better compounds tend to have higher *c*log *P* values (∼>4.3).

To ensure that compounds were inhibiting PI3K signaling in cells, compound **19** was tested for p-Akt (at Thr308) inhibition in PC-3 human prostate cancer cells. Immunostaining for phosphorylated 4E binding protein 1 (p4EBP1) was also conducted as a marker of pathway inhibition downstream of mTOR (Fig. 3). p-Akt inhibition is seen starting at 0.3 μM and is complete at 3 μM. Densitometer assessment of the p-Akt inhibition blots indicates an

Table 4
Cellular proliferation inhibition of selected benzofuran-3-one indoles

Compd	PI3K-α IC_{50}[a] (nM)	mTOR IC_{50}[a] (nM)	Caco IC_{50}[a] (μM)	LoVo IC_{50}[a] (μM)	PC3 IC_{50}[a] (μM)	*c*log *P*
13	3	3	9.0	3.6	4.0	4.19
19	2	9	2.1	1.2	0.8	5.80
20	1	1	7.5	4.7	1.9	4.38
23	7	4	7.2	2.5	1.3	4.70
28	9	18	2.8	1.7	1.8	4.82
29	11	9	2.0	2.3	1.5	4.67
30	5	11	4.7	2.2	2.4	3.74
31	4	7	9.0	5.9	6.9	3.20
35	5	118	9.3	5.7	2.8	5.07
36	8	18	4.7	4.6	2.4	5.03
37	15	153	10.0	7.5	9.5	4.10
38	7	108	10.0	10.0	10.0	3.57

[a] Values are means of two experiments; standard deviation is ±10%.

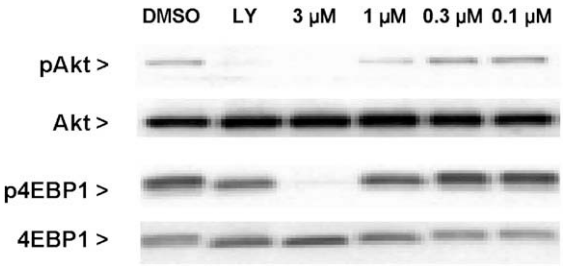

Figure 3. Inhibition of PI3K signaling in PC-3 cells. PC-3 cells were treated with DMSO, 10 μM LY 294022 (positive control) or the indicated doses of **19** after 6 h. Protein lysates were prepared and immunoblotted for phospho-Akt T308 (p-Akt (T308)) and phosphorylated 4E binding protein 1 (p4EBP1).

IC_{50} = 385 nM. Suppression of p-Akt is indicative of inhibition of cellular PI3Ks which are upstream of KT in the PI3K signaling pathway.

In conclusion, we have presented a series of the benzofuran-3-one indole PI3K inhibitors identified via HTS efforts. Structure based design with a PI3K-α homology model derived from a PI3K-γ X-ray structure led to compounds with improved selectivity, solubility and CYP inhibition. Our hit to lead optimization has identified potent PI3K-α inhibitors with good selectivity versus PI3K-γ and mTOR. This scaffold has also provided dual PI3K-α/mTOR inhibitors with good selectivity over PI3K-γ. Compounds showed activity in various cellular proliferation assays with signaling through the PI3K pathway confirmed via phospho-Akt inhibition in PC-3 cells. This lead series provides the basis for developing more potent, novel inhibitors of the PI3K signaling pathway with the desired selectivity profile.

References and notes

1. Vanhaesebroeck, B.; Leevers, S. J.; Ahmadi, K.; Timms, J.; Katso, R.; Driscoll, P. C.; Woscholski, R.; Parker, P. J.; Waterfield, M. D. *Annu. Rev. Biochem.* **2001**, *70*, 535.
2. Liu, P.; Cheng, H.; Roberts, T. M.; Zhao, J. J. *Nat. Rev. Drug Disc.* **2009**, *8*, 627.
3. Saal, L. H.; Holm, K.; Maurer, M.; Memeo, L.; Su, T.; Wang, X.; Yu, J. S.; Malmstrom, P. O.; Mansukhani, M.; Enoksson, J.; Hibshoosh, H.; Borg, A.; Parsons, R. *Cancer Res.* **2005**, *65*, 2554.
4. She, Q. B.; Solit, D.; Basso, A.; Moasser, M. M. *Clin. Cancer Res.* **2003**, *9*, 4340.
5. Wee, S.; Lengauer, C.; Wiederschain, D. *Curr. Opin. Oncol.* **2008**, *20*, 77.
6. Ameriks, M. K.; Venable, J. D. *Curr. Top. Med. Chem.* **2009**, *9*, 738.
7. Tsang, C. K.; Qi, H.; Liu, L. F.; Zheng, X. F. S. *Drug Discovery Today* **2007**, *12*, 112.
8. Gilbert, A. M.; Nowak, P.; Brooijmans, N.; Bursavich, M. G.; Dehnhardt, C.; Santos, E. D.; Feldberg, L. R.; Hollander, I.; Kim, S.; Lombardi, S.; Park, K.; Venkatesan, A. M.; Mallon, R. *Bioorg. Med. Chem. Lett.* **2010**, *20*, 636.
9. Venkatesan, A. M.; Dehnhardt, C. M.; Chen, Z.; Santos, E. D.; Dos Santos, O.; Bursavich, M.; Gilbert, A. M.; Ellingboe, J. W.; Ayral-Kaloustian, S.; Khafizova, G.; Brooijmans, N.; Mallon, R.; Hollander, I.; Feldberg, L.; Lucas, J.; Yu, K.; Gibbons, J.; Abraham, R.; Mansour, T. S. *Bioorg. Med. Chem. Lett.* **2010**, *20*, 653.
10. All newly prepared compounds were characterized by ^{1}H NMR and reversed phases-HPLC/MS spectroscopy.
11. Gastpar, R.; Goldbrunner, M.; Marko, D.; von Angerer, E. *J. Med. Chem.* **1998**, *41*, 4965.
12. Tanaka, M.; Kaneko, T.; Akamatsu, H.; Okita, M.; Chiba, K.; Obaishi, H.; Sakurai, H.; Yamatsu, I. *Eur. J. Med. Chem.* **1995**, *30*, 179.
13. Teo, C. C.; Kon, O. L.; Sim, K. Y.; Ng, S. C. *J. Med. Chem.* **1992**, *35*, 1330.
14. Yu, K.; Toral-Barza, L.; Discafani, C.; Zhang, W. G.; Skotnicki, J.; Frost, P.; Gibbons, J. J. *Endocr. Relat. Cancer* **2001**, *8*, 249.
15. de la Mora, M. A.; Cuevas, E.; Muchowski, J. M.; Cruz-Almanza, R. *Tetrahedron Lett.* **2001**, *42*, 5351.